Modelling and simulation of the electrical resistance sintering process of iron powders

J.M. Montes[1], F.G. Cuevas[2], F.J.V. Reina[1], F. Ternero[1], R. Astacio[1], E.S. Caballero[1], J. Cintas[1]

[1] *Metallurgy and Materials Engineering Group*
Escuela Técnica Superior de Ingeniería, Universidad de Sevilla
Camino de los Descubrimientos, s/n, 41092 Sevilla, Spain

[2] *Department of Chemical Engineering, Physical Chemistry and Materials Science*
Escuela Técnica Superior de Ingeniería, Universidad de Huelva
Campus El Carmen, Avda. 3 de Marzo s/n, 21007 Huelva, Spain

Corresponding author: F. Ternero, Tel.: +34 954487305, e-mail: fternero@us.es

Abstract. In this paper, the process known as *Electrical Resistance Sintering under Pressure* is modelled, simulated and validated. This consolidation technique consists of applying a high-intensity electrical current to a metallic powder mass under compression. The Joule effect acts heating and softening the powders at the time that pressure deforms and makes the powder mass to densify. The proposed model is numerically solved by the finite elements method, taking into account the electrical-thermal-mechanical coupling present in the process. The theoretical predictions are validated with data recorded by sensors installed in the electrical resistance sintering equipment during experiments with iron powders. The reasonable agreement between the theoretical and experimental curves regarding the overall porosity and electrical resistance suggests that the model reproduces the main characteristics of the process. Also, metallographic studies on porosity distribution confirm the model theoretical predictions. Once confirmed the model and simulator efficiency, the evolution of the temperature and the porosity fields in the powder mass and in the rest of elements of the system can be predicted. The influences of the processing parameters (intensity, time and pressure) as well as the die material are also analyzed and discussed.

Keywords*:* powder metallurgy; field-assisted sintering techniques; electrical resistance sintering; modelling; finite elements method; COMSOL

1. Introduction

Techniques using electricity as a means of sintering powders (both metals and ceramics) are known as FAST (of *Field-Assisted Sintering Techniques*). According to the acronym, the main characteristic and common factor among them, and one of the main difference with respect to the

conventional route of cold pressing and furnace sintering, is the speed. This high speed supposes an important advantage, frequently making unnecessary the use of vacuum or inert atmospheres. Another advantage of the FAST techniques is the production of parts with net or near-net shapes. Although grouped under a common name, the physical phenomena in the different FAST modalities are quite different. The differences are mainly due to: a) the type of the power source, b) the nature of the die containing the powders (conductive or insulating) and c) the process dwelling (from minutes to microseconds). Obviously, in addition to these characteristics, the nature and the electric conducting character of the powder to be sintered is of great importance.

The development of the different modalities of electrical sintering has been detailed reviewed by Grasso *et al.* [1]. In 1906, Lux [2] registered the first patent on powder sintering using direct current. The main purpose of his invention was the industrial scale production of filaments for incandescent lamps by compacting tungsten or molybdenum particles. In 1913, Weintraub and Rush [3] patented a modified sintering method that combined electrical current with pressure. The benefits of this method were tested by sintering refractory metals, as well as conductive carbide or nitride powders. Taylor [4] described in 1933 the *Electrical Resistance Sintering (ERS)* process, one of the FAST techniques, although it was around 1955 when Lenel [5] carried out a systematic study.

The ERS process has technically improved from then, but its requirements remain virtually the same. Basically, this technique requires a low-voltage and high-intensity alternating current at the time that pressure is applied. The current is forced to pass through the powder mass by using an insulating die. The thermal energy released by the Joule effect softens the powders as a result of the temperature increase, and together to the mechanical load, induce powder densification. The electrical requirements coincide with those of a resistance welding equipment, which can be used to implement the ERS technique. The typical duration of the ERS process is approximately 1 s.

In other FAST modality known as *electrical discharge consolidation (EDC)*, also a high intensity current passes through the powder mass [6-9], but the voltage can reach much higher values than in ERS. The energy stored in a bank of capacitors can produce this combination of high intensity and high or moderately high voltage. The micro-weldings at particles contacts produced by the high energy in the capacitors allows the use of an extraordinarily short consolidation time, in the order of the milliseconds, or even microseconds. The higher applied voltage with respect to the ERS technique makes possible to sinter highly resistive initial powders because of the remarkable intensity of the current passing through the powder aggregate. However, the achieved densification is often quite lower than that obtained by other FAST modalities.

Perhaps, the most widely studied FAST modality is *Spark Plasma Sintering* (*SPS*), where a pulsed DC current passes through a conductive graphite die, as well as through the powder mass, in case of conductive samples. This makes possible a heating rate of up to 1000 K/min, resulting in a sintering process typically lasting a few minutes. The process produces high densified samples in lower times than those required in conventional PM, and can be applied to non-conductive powders (something not possible with the two aforementioned FAST modalities). An extensive review about SPS works can be found in the recent works by R. Orrù *et al*. [10] and O. Guillon *et al.* [11].

Although experimentally tested for many years, the theoretical studies of FAST techniques are very limited. Some of the first studies [12-19] come from the former USSR, with more recent advances being carried out in the context of the SPS technique [20-27]. A theoretical one-dimensional model of ERS technique can be found in [28].

Because of the technical differences between SPS and ERS, mainly due to the electrical conductivity of the die and the process duration, many theoretical advances of the SPS process cannot be transferred to describe the ERS process. Even the models validation strategies with experimental practices cannot be the same. For instance, the global temperature evolution can be known in SPS by placing thermocouples in the external frontiers of the compact, however, due to the extraordinary shortness of ERS process, the thermal inertia of the sensors makes it impossible, being the problem worsen because of the heterogeneous temperature distribution inside the compact in the ERS modality.

Moreover, the inexistence of equations that adequately describe the thermal, electrical and mechanical behaviours of powder aggregates, makes most models to be uncompleted, ignoring relevant aspects. Most models are based on spherical particles with ordered arrangements, which is only valid for small porosity levels. On the other hand, the presence of very thin oxide layers surrounding metallic particles complicate the description of the global properties of the powder aggregate, mainly those of an electrical nature.

In this paper, a theoretical model to describe the ERS process will be proposed. This model will help knowing experimentally inaccessible variables inside the powder aggregate (i.e., temperature, porosity and densification rate), as well as selecting suitable experimental conditions, such as current intensity, processing time, external pressure, and even the ideal materials for the die.

Equations modelling the behaviour of the powders and die, the differential equations governing the heat generation, heat transmission and the powder densification, and the strategies for tackling the resolution of the model through the finite elements method will be discussed. The model predictions will be validated with the results obtained in ERS experiments carried out with

iron powder (chosen because of its evident technological interest). A resistance welding equipment conveniently adapted and instrumented, with the modern medium frequency technology was used.

2. Modelling and simulation

The theoretical study of the system evolution requires knowing how the heat is generated and flows through the system, and how the powders densify with time. This densification is due to the applied pressure and the thermal energy generated by Joule effect in the powder mass, resulting in a strong thermomechanical coupling. Thus, properties of the powders aggregate will depend on temperature and porosity, and therefore two time-based variations should be considered.

Solving this problem should allow to know at any time: (i) the temperature distribution in the whole system, (ii) the porosity distribution of the powder mass and (iii) the global properties of the compact (height, porosity and electrical resistance).

2.1. Geometry and working conditions

Essentially, the system to be modelled consists of a metallic powder mass enclosed between two electrodes of section S_N, all surrounded by an electrically insulating die. The geometry of the system (with axial symmetry) is schematically shown in Fig. 1.

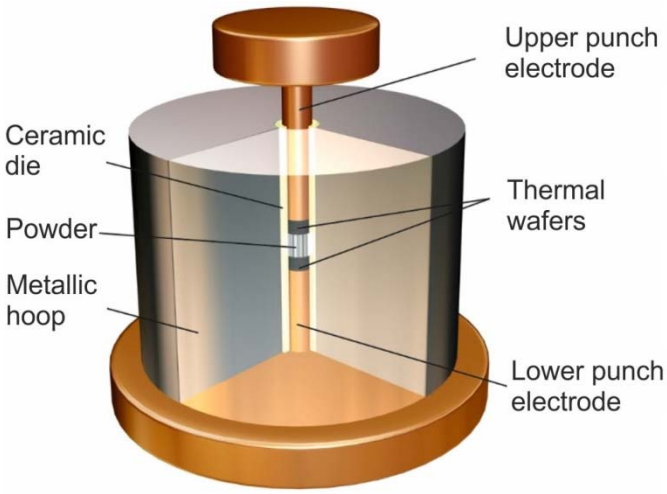

Figure 1. Scheme of the system geometry. Both electrodes lie on water cooled bedplates.

Replaceable thermal wafers, with thermal and electrical conductivities some lower than the electrodes themselves, are placed in direct contact with the powders to avoid thermal leaks and electroerosion of the electrodes.

The sequence of an ERS experiment (Fig. 2) consists of an initial stage of *cold-pressing*, always lasting 1000 ms, with a constant force (F) and no current passing through the powder. The

following stage consists on *heating and pressing*, in which the same force continues applied at the time that the electrical current starts flowing through the powders. During the later stage of *cooling/forging*, lasting 300 ms, the force is maintained and again no current passes through the powders. The nominal pressure results in $P_N = F/S_N$.

In addition, because of the technical characteristics of the ERS equipment, the current intensity passing through the system (I_0) can only be regulated when the desired value is approached by an increasing ramp. Thus, the effective current intensity passing through the system depends on time according to:

$$I(t) = \begin{cases} 0 & if \quad 0 \le t \le t_0 \\ I_0 \left(\dfrac{t - t_0}{t_S - t_0} \right) & if \quad t_0 < t \le t_S \\ I_0 & if \quad t_S < t \le t_C \\ 0 & if \quad t_C < t \le t_T \end{cases} \tag{1}$$

where t_0 represents the end of the cold-pressing period, t_S the start of the constant intensity, t_C the end of the heating period, and t_T the end of the process.

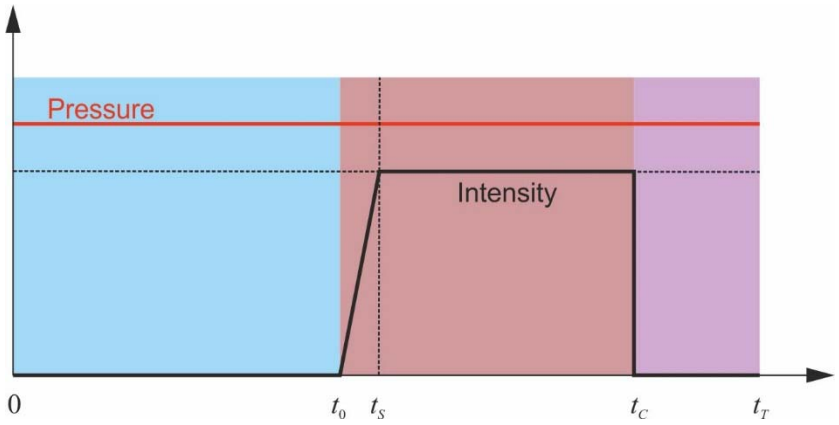

Figure 2. Typical sequence in an ERS process, showing the current intensity passing through the system and the applied pressure. In all the experiments, the cold-compaction and cooling/forging periods lasted 1000 and 300 ms, respectively.

2.2. Materials properties

The properties of a system with a certain porosity are known to depend on the level of porosity, defining the so-called effective properties, p_E. This dependence is not always considered in the different FAST modelling studies. Clearly established expressions include those for the apparent density [29], which is indeed a direct measure of the porosity, and the specific heat of a porous material [30]. However, the dependence of the electrical resistivity and the thermal conductivity is

a more complex matter, mainly because these properties depend on the powder particles morphology [31-36]. Taking into account these dependences, the equations used in this work are of the form $p_E = p_m \cdot f(\theta/\Theta_M)$, where p_E is the effective value of the property, p_m is the corresponding property for the bulk material, and $f()$ represents a function of θ, the porosity, and Θ_M, the tap porosity of the powder, an upper limit of the porosity obtained after powder vibration [37]. Thus, these equations are valid in the whole physical range of the porosity, allowing the proposed model to describe the consolidation of both loose and pre-compacted powders.

Moreover, the initial value of the electrical resistance of a powders aggregate has an added difficulty which has received a limited attention. As reported in [38-43], this initial resistance is much related to the oxide layer surrounding powder particles.

Thus, we will assume that the effective properties (density, γ; specific heat, c; electrical resistivity, ρ; and thermal conductivity, k) of any volume of the powder aggregate depend on its local porosity (θ) as follows [40]:

$$\gamma = \gamma_m(1-\theta) \tag{2}$$

$$c = c_m \tag{3}$$

$$\rho = \rho_{res}\left(1-\theta/\Theta_M\right)^{-n} \tag{4}$$

$$k = k_m\left(1-\theta/\Theta_M\right)^{\frac{3}{2}} \tag{5}$$

where γ_m, c_m and k_m are the corresponding properties of the bulk material. The parameter ρ_{res} is the residual resistivity and does not coincide with ρ_m (the bulk resistivity of metal) due to the presence of oxide coating the powder particles. The dimensionless exponent n models the oxide descaling process of the powder particles during compaction [40].

In addition to its dependence on porosity, materials properties do also depend to a greater or lesser extent on temperature. Thus, we will assume that the thermal and electrical properties of the powders, punches and die (all considered as bulk materials) depend on the temperature:

$$c_m = c_m(T),\ k_m = k_m(T), \text{ and } \rho_m = \rho_m(T) \tag{6}$$

The exact dependence is modelled according to the internal COMSOL properties library, using interpolation by cubic splines from tabulated data. (The thermal expansion of the different materials during the process has been neglected due to its little influence on the final results.)

Because of temperature changes, the powder could suffer phase transformations, which should also be considered. Thus,

$$c_m(T) = \varsigma_m(T) + \sum_i \delta_D(T - T_i) \cdot L_i \tag{7}$$

where ς_m is the specific heat itself, L_i are the different latent heats of the corresponding phase transformations at the temperatures T_i, and δ_D is the Dirac delta function, which can be approached for numerical purposes by:

$$\delta_D\left(T - T_t\right) \approx \frac{1}{\varepsilon\sqrt{\pi}} \exp\left(-\left(\frac{T - T_t}{\varepsilon}\right)^2\right) \tag{8}$$

where T_t is the temperature of the phase transition and ε is a small quantity that represents the semi-width of the curve. This numerical implementation is flexible enough (through the variation of the parameter ε) to guarantee the adequate numerical convergence.

Regarding the electrical resistivity of the oxide layer covering the metallic particles, ρ_x, its thermal dependence must be considered, being modelled according to the analytical function $\rho_x(T) = A_x \exp\left(E_x/(2RT)\right)$ [44]. As shown in [40], the following similar expressions is proposed for ρ_{res} and n:

$$\rho_{res}(T) = \rho_m(T) \exp\left(T_\rho/T\right) \tag{9a}$$

$$n(T) = \tfrac{3}{2} \exp\left(T_n/T\right) \tag{9b}$$

where T_n and T_ρ are two convenient temperatures related to the activation energies of the descaling process of the powder.

2.3. The mechanical problem

During the cold pressing stage, acting a nominal pressure P_N, the powder porosity is reduced from the tap porosity Θ_M to the initial value during current passing, Θ_0. This initial value can be modelled according to different equations [45, 46], being selected in this work the Secondi equation [47] because of its simplicity. This equation is expressed in terms of porosity as:

$$\Theta_0 = \Theta_\infty + \left(\Theta_M - \Theta_\infty\right) \exp\left(-\left(P_N/a\right)^b\right) \tag{10a}$$

The values of the empirical parameters Θ_∞, a and b are obtained by fitting by least square regression the experimental compressibility curve of the powders [48], obtained previously to the

ERS experiences, to the Secondi expression. In this fitting process the value of Θ_M is fixed to that obtained experimentally. Thus, after the cold-pressing stage, the powder column reaches a porosity Θ_0, a height H_0 and it exhibits an electrical resistance R_0, given by:

$$H_0 = M/\left(S_N(1-\Theta_0)\gamma_m\right) \tag{10b}$$

$$R_0 = \rho_0 H_0 / S_N \tag{10c}$$

where M is the powder mass, and ρ_0 is the resistivity for the porosity Θ_0.

During the heating and cooling stages, the porosity associated to each elemental or local volume (a finite element) at the domain of the powder mass is further reduced according to the following law [49], obtained from the Norton creep law adapted to a porous material and a much quicker deformation mechanism as that produced by high temperature under applied pressure:

$$\boxed{\frac{d\theta}{dt} = -\frac{A_c}{T}(1-\theta)\left(\frac{2}{\sqrt{3}}\frac{\sigma_{eq}}{E_m}\cdot\frac{\sqrt{\theta/\Theta_M}}{1-\theta/\Theta_M}\right)^{n_c}\cdot\exp\left(-\frac{Q_c}{RT}\right)} \tag{11}$$

where θ is de local porosity, T the local absolute temperature and σ_{eq} is the local equivalent stress (the Von Misses tension) responsible for the powder deformation and densification, and depending on the value of P_N. Regarding parameters from the fully dense material, E_m is the Young modulus at room temperature (a fix value, added for the sole purpose of making the quotient σ_{eq}/E_m dimensionless), A_c is the pre-exponential factor in the Norton creep law, and n_c and Q_c are the creep exponent and the creep activation energy, respectively [50]. R the ideal gas constant. The initial condition for the porosity, at the start of the heating stage, for the whole volume occupied by the powder is $\theta(t = t_0) = \Theta_0$.

2.4. The thermal problem

The thermal problem requires considering the heat generated by Joule effect, but also solving the partial differential equation of heat transfer by conduction, described elsewhere, for instance by Tijonov and Samarski [51] or Haberman [52]. Heat transfer by convection will be neglected given the small fraction that the pores represent, and its small contribution relative to conduction. Similarly, radiation is considered negligible given the low global temperature reached, and the short time at high temperatures in particular points [53].

When a powder mass is traversed by a current intensity I, the temperature throughout the system is computed by solving the following thermal problem:

$$\boxed{\frac{\partial}{\partial t}(\gamma c T) = \vec{\nabla}\left(k\vec{\nabla}T\right) + \frac{I^2\rho}{S_N^2}} \tag{12a}$$

where the coefficients γ(density), c (specific heat), k (thermal conductivity) and ρ (electrical resistivity) are functions that, in general, depend on the position and temperature. The problem has to be completed with the initial condition:

$$T(\vec{r}, t = t_0) = T_0 \text{, in all the system} \tag{12b}$$

and the following boundary condition, related to the cooling effect of the electrodes, always at a fix temperature T_c:

$$T(t) = T_c \text{, at the electrodes base in contact with the bedplates at any time} \tag{12c}$$

2.5. Global properties

Integrating the local properties in the whole volume occupied by the powder should result in the global properties of the compact at any moment. Thus, during the heating and cooling stages ($t_0 < t \leq t_T$), the compact global properties evolve as follows:

$$\Theta(t) = \frac{1}{V_P}\int_{V_P} \theta(t)dV \tag{13}$$

$$\mathrm{H}(t) = \frac{M}{S_N \gamma_m \left[1 - \Theta(t)\right]} \tag{14}$$

$$\mathrm{T}(t) = \frac{1}{V_P}\int_{V_P} T(t)dV \tag{15}$$

$$\mathrm{R}(t) = \frac{\mathrm{H}(t)}{S_N V_P}\int_{V_P} \rho(t)dV \tag{16}$$

$$\eta(t) = \frac{1}{M}\int_{t_0}^{t} I^2(t)\cdot \mathrm{R}(t)dt \tag{17}$$

where Θ is the instant global porosity, H is the instant compact height, M is the powder mass, T is the instant mean temperature, R is the instant global electrical resistance and η is the cumulative thermal energy generated per unit mass. V_P is the instantaneous volume and S_N the cross-sectional area of the powder column.

2.6. Numerical resolution with COMSOL Multiphysics

When finite elements are used to solve a model in a system with a geometry that varies with time, fixed meshes are not a good option. However, deforming meshes (deformed in COMSOL nomenclature) can adequately reproduce the system deformation, as is the case of this work because of to the densification of the powder.

The geometry of the system to be modelled in this work embraces a domain with a deformed and other with a fixed mesh, the former corresponding to the moving parts of the system (upper electrode and wafer and powder), and the latter to the domain whose geometry is fixed. Fig. 3a shows these two domains.

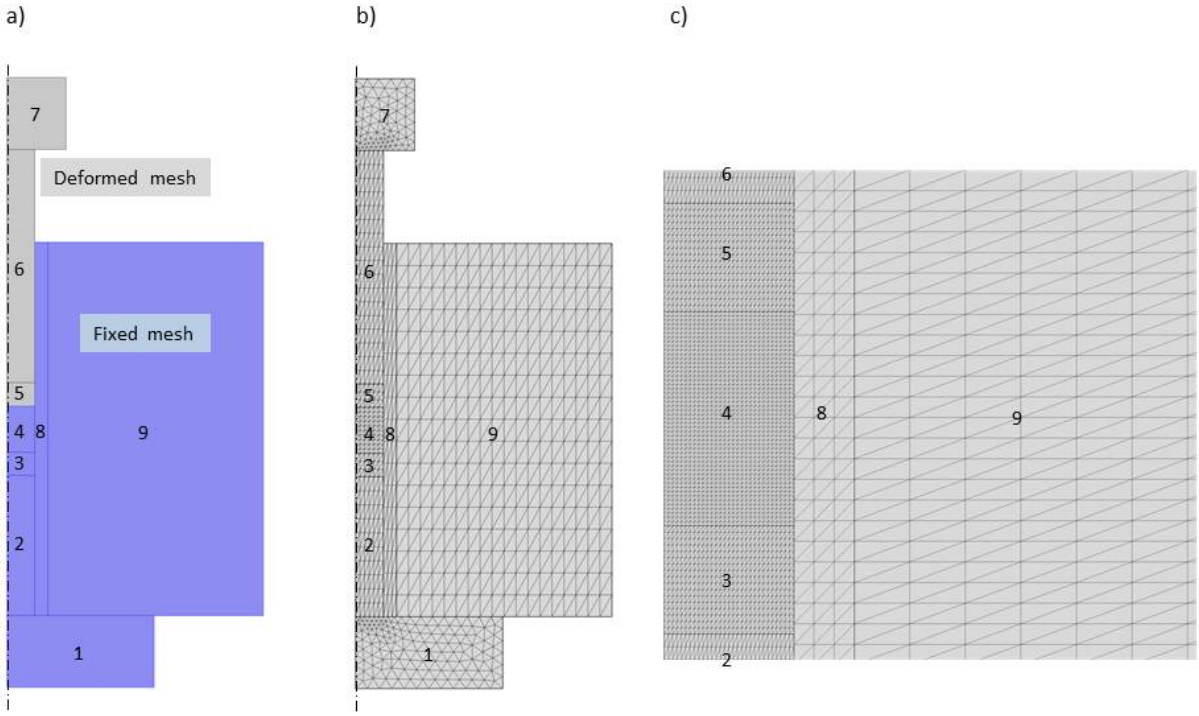

Figure 3. (a) System showing the domains studied with deformed and fixed meshes. Parts numbered with 1, 2, 6 and 7 represent the punches, 3 and 5 the wafers, 8 and 9 the die and hoop and 4 the powder mass. (b) Mesh details used in this work. (c) Amplified detail of the system.

The fixed mesh works with fixed finite elements. The deformed mesh, however, requires setting its boundaries and displacements with respect to the fixed mesh. This is easier established for the upper punch and wafer, in which vertical movements of the mesh will only be allowed. Both triangular and rectangular finite elements have been used, the later to take advantage of the system axial symmetry (Fig. 3b).

It was considered that the subsystem formed by the upper punch, the upper wafer and the powder forms a Boolean union. The subsystem formed by the remaining parts forms a different union. These two systems interact through an operation called in COMSOL “Assembly union”,

which carries out the link between subsystems with can suffer relative movement, without generating stresses between them. The type of contact chosen has been “identity pairs” because there is no separation at any moment between the subsystems. In order to allow the movement of the former subsystem, discretization was carried out with a deformed mesh.

A mesh sensitivity analysis was carried out in order to define the adequate number of finite elements, reaching a compromise value when relative discrepancies of porosity and average temperature in the final instant of the MF-ERS process were less than 1% among the different simulations. The final mesh consisted of a total of 9667 nodes of triangular elements with linear form functions. The size of the elements resulted to be about 0.2 mm in the powder, punches and wafers, being some bigger in the die and hoop (approx. of 1 mm).

Because of the complexity of the system simulation, it was considered that all the intervening materials exhibited a non-linear elastic behavior, and because of the high deformations suffering the powder, a non-linear analysis in terms of displacement and deformations is needed.

The creep phenomenon, only present in the powder domain, is modeled by the ordinary differential equation in Eq. (11). The resolution of this ODE was carried out externally through the physics called in COMSOL “Domain ODEs and DAEs”.

In order to solve the model, COMSOL will be required to compute the global porosity of the powder mass for every moment of the process, through computing the porosity variation of each finite element for each instant, with help of Eq. (11). However, COMSOL cannot directly change the volume of the finite element according to the new porosity, because of the big resulting strains. It is therefore necessary to calculate the integral average of the local porosity (θ) in all the compact. This mean porosity is the overall or global porosity (Θ). Also, the new height of the powder column (H) is related to the overall porosity of the powder from Eq. (14), and finally the powder/electrode interface is relocated and the mesh automatically deformed by COMSOL. This has been an enforced strategy because all the tests carried out with plastic or viscoplastic mechanical behaviours have failed to converge with so much severe deformations (even after consulting with technical assistance from COMSOL). Apart of the geometrical considerations, the ‘physics’ or moduli of solid mechanics, heat transfer and electric current moduli need to be linked. Also the differential equations solving module is necessary for the calculation of the porosity. All of them will take advantage of the 2D axial symmetry of the system. On the other hand, continuous values of the different variables in the entire model must always be reached.

Moreover, a maximum time between two simulated steps was defined in COMSOL to reduce relative discrepancies below 1%. Backward Differentiation Formulas (BDF, a method to increase the accuracy of the approximations of time derivatives using results from previous computed times) were also enabled to reduce the time step in case of difficultness in convergence. Time

steps below 5 ms do not significantly alter the final results, but longer times make the simulation not to converge. The tolerance allowing convergence for voltage, porosity and displacements was set to 0.001, and 0.01 for the temperature.

Finally, Newton method for solving each independent problem has been chosen, due to their clear non-linear behaviour.

With the aforementioned conditions, the computational time of a complete simulation is of the order of one hour.

3. Experimental procedure and validation

3.1. The Electrical Resistance Sintering equipment

Electrical Resistance Sintering (ERS) equipments are not commercialized. Nevertheless, the requirements of high intensity and low voltage, and the application of the necessary load to press the powders, are adequately satisfied by a resistance welding machine. One of these equipments (Serra Soldadura S.A., Spain) consisting of a 100 kVA three-phase transformer, servodrived heads of 15 kN, and electronic control of the process sequences, has been used in this work. Because of the medium frequency (1000 Hz) technology of the equipment, the technique will be denominated Medium Frequency ERS (MF-ERS). Follow-up sensors allow monitoring the displacement of the mobile electrode, the applied load and the efficient current voltage and intensity.

Dies constitute one of the main problems in ERS experiments. Good mechanical properties and electrical and thermal insulating properties are required. In this work, an alumina tube (16 mm of outer and 12 mm of inner diameter) is used. (For selected experiences, a sialon tube was used, in order to compare the effect of the die material.) Powders inside the die are in direct contact with electro-erosion resistant wafers (75.3%W-24.6%Cu), and these with heat-resistant copper electrodes (98.9%Cu-1%Cr-0.1%Zr). The wafers, with a relatively low thermal conductivity, dampen the heat flow from the powder mass towards the electrodes (in contact with water-cooled bedplates).

Knowing the mass and the final height of de compact, the *global porosity* can be known at any moment of the MF-ERS process through the registered information of the upper electrode position (by insulating Θ from Eq. (14) applied to the experimental values, once known the compact height at any moment of the process). On the other hand, the *electrical resistance* of the powder mass during the different stages of an MF-ERS experiment can also be known by processing, from the sensor data, the voltage between the electrodes and the circulating current intensity.

3.2. Consolidation experiences

MF-ERS experiments were carried out with Fe WPL200 water atomised iron powder from *QMP Metal Powders GMBH* (approx. 3.5 g), with a purity of 99.4% and main impurities of 0.2% Mn, 0.2% O, 0.01% C and 0.009% S. The absolute density of the powder is 7.87 g/cm^3 and its tap density 2.79 g/cm^3 [37], resulting a mean particle size of 84.4 μm from laser diffraction. Fig. 4 shows a scanning electron microscopy (SEM) micrograph of the powder.

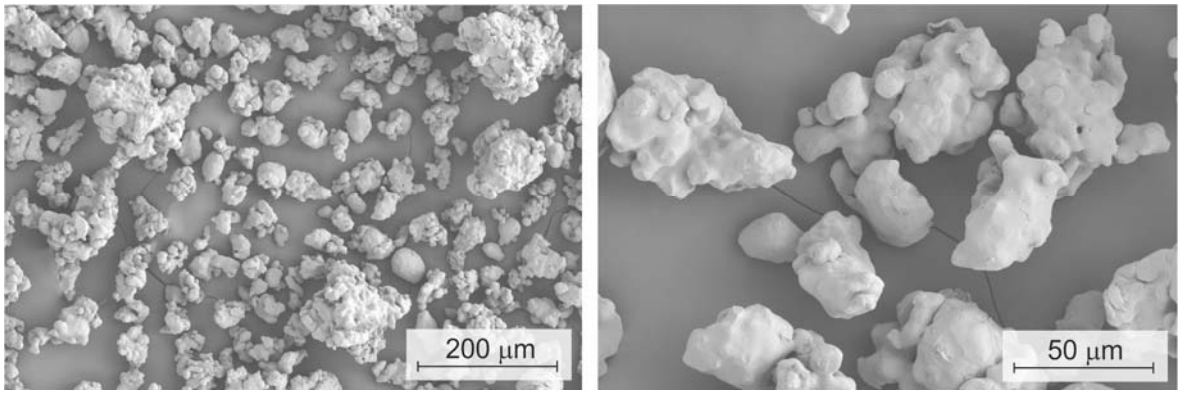

Figure 4. SEM micrographs of the Fe WPL200 powders used in the MF-ERS experiments.

Consolidation experiences were carried out with pressure being applied 1000 milliseconds before the application of current (i.e., t_0 in Fig. 2 is 1000 ms). The applied current varied among 6, 8 and 10 kA (current densities between 5.3 and 8.8 kA/cm^2) with current passing for 400, 700 and 1000 ms, and a final period of 300 ms in which only again pressure was applied. The system evolution and the final densification was studied with regard to the current intensity and time. More severe conditions, mainly intensities higher than 10 kA and times in the order or higher than 1000 ms, resulted in compacts welded to the wafers.

The applied load during the whole MF-ERS process resulted in a pressure of 100 MPa in most cases (200 MPa for selected experiences). Lower pressures do not guarantee current passing in all the experiments, with higher ones deteriorating the die after just a few experiences.

With the aim of comparing the porosity obtained in conventional and electrical sintered compacts, 12 mm diameter compacts were prepared through a cold-press and furnace-sinter process. Several processing conditions were tested, finally selecting a pressure of 500 MPa after die-wall lubrication, and sintering in vacuum at 1175 ºC for 30 min. The final porosity of the compacts was near 15 %.

3.3. Strategy of validation

The equations in the model need to be feed with the parameters values. Some of these values can easily be found in the literature. Such is the case of the thermal dependences of all the materials in the system [54-56] or the creep activation energy Q_c in Eq. (11), which is consider to be 193

kJ/mol [54]. (This value represents the 80% of the self-diffusion energy of the pure iron, according to Evans and Wilshire [50]).

Other parameters values can be known by fitting experimental data. The values of T_n and T_ρ in Eq. (9a) and Eq. (9b) were obtained by fitting the experimental resistivity-porosity curve of the powder, resulting in T_n = 225.792 K and T_ρ = 881 K, as described in [40].

Similarly, the values of the parameters in the Secondi equation (obtained by fitting to the compressibility curve [48]) were Θ_∞ = 0.016, Θ_M = 0.645, a = 304.9329 MPa and b = 0.7967, as described in [40]. Finally, other parameters as T_0 and T_c in Eqs. (12) are fixed to 21 ºC.

On the other hand, the model considers two fitting parameters, whose values are difficult to measure and know. These parameters are A_c and n_c, (Eq. (11)), which control the creep densification rate. Their values are chosen by the COMSOL optimization modulus, by comparing the simulated and experimental evolution of the compact global porosity for a particular experiment (in this case, 100 MPa, 10 kA and 1000 ms of heating). Once the values of A_c and n_c are fixed from this particular experiment ($A_c = 10^{46}$ and n_c = 6.8), they will be considered constant for any other experiments carried out with the same powder under different processing conditions (different pressure, current dwelling time and/or current intensity, and die material). The model will be considered valid if the theoretical predictions for those new situations reasonably agree with the experimental data.

With the simulator, it is possible to carry out virtual experiments in order to verify the influence that the different process parameters have on the final results. Some of these parameters will be studied in the following sections.

4. Results and discussion

4.1. Final Porosities and Specific Thermal energies

Table 3 shows the values of the final porosity (Θ_F) and the specific thermal energy (η) released in each experiment and the corresponding final values obtained in each simulation. As expected, higher intensities and/or current passing times produce a more densified material, because of the higher energy released. MF-ERS experiments reach a significant densification, from a green or as-pressed porosity of 0.43, a final porosity of 0.30 is achieved with the lighter conditions, and 0.06 by using the tougher parameters.

Table 3. Experimental and simulated values of the final porosity (Θ_F) and cumulative specific thermal energy (η) for all the sintering conditions.

	Θ_F (experimental)	Θ_F (simulated)	η [kJ/g] (experimental)	η [kJ/g] (simulated)

6 kA – 400 ms	0.30	0.31	0.35	0.25
6 kA – 700 ms	0.28	0.27	0.47	0.37
6 kA – 1000 ms	0.24	0.25	0.59	0.47
8 kA – 400 ms	0.19	0.21	0.43	0.34
8 kA – 700 ms	0.16	0.17	0.60	0.49
8 kA – 1000 ms	0.13	0.14	0.77	0.62
10 kA – 400 ms	0.12	0.12	0.53	0.43
10 kA – 700 ms	0.08	0.08	0.72	0.62
10 kA – 1000 ms	0.06	0.05	1.02	0.90

The average discrepancy between the measured and simulated Θ_F values is under 10%, which can be considered a good result. However, predictions of the specific thermal energy (η) differ much more with respect to the measured values. The reason for this is the way to determine the experimental and simulated values. Both are determined through Eq. (17) by time integrating $I^2 \cdot R$. However, the experimental value of R at each instant cannot be determined directly, but it has to be determined from the monitored values of current intensity (I) and voltage measured between the equipment bedplates in contact with the electrodes (V) at each instant. Voltage drop due to the powder column ($I \cdot R$), and the corresponding value of R, is computed by detracting to V the voltage drop in electrodes and wafers (which are computed by multiplying the intensity by the respective resistances at room temperature, which are supposed constant).

Thus, the experimental values of η include the thermal energy released by the powder mass, and also partially by the electrodes and wafers (whose respective resistances increase with respect to the considered value because of the increase in temperature), and by the effect of different contacts (between electrodes, wafers and the powder mass). In order to obtain the simulated values gathered in Table 3, the contribution of electrodes and wafers was subtracted, but it is difficult to quantify the effect of the contacts. By comparison the experimental and simulated values of η, a mean discrepancy of 0.11 kJ/g is observed, which therefore could be attributed to the effect of the temperature on the resistance of the punches and the contacts between different parts of the system. By subtracting this amount from the experimental values, it can be shown that the results match reasonably well with the simulated ones.

Fig. 5 gathers macrographs of diametrical sections of the MF-ERS compacts, and the corresponding porosity distribution maps from the final instant of the simulations. As compared to the also shown relatively uniform porosity distribution in conventional sintered compacts, electrically consolidated specimens are characterized by a heterogeneous porosity distribution, with a periphery more porous than the center. This heterogeneity is produced by a heterogeneous temperature distribution, with a minimum value near the electrodes and die walls and increasing

towards the center of the specimen (the electrodes are refrigerated and the die acts as a heat sink). Macrographs show how the porosity (black dots) decreases with increasing time and/or intensity. On the other hand, the clear symmetry of the simulated images differ of the random porosity distribution in real experiences, mainly for low intensities and dwelling times, despite the global porosity reasonably agrees between experiments and simulations.

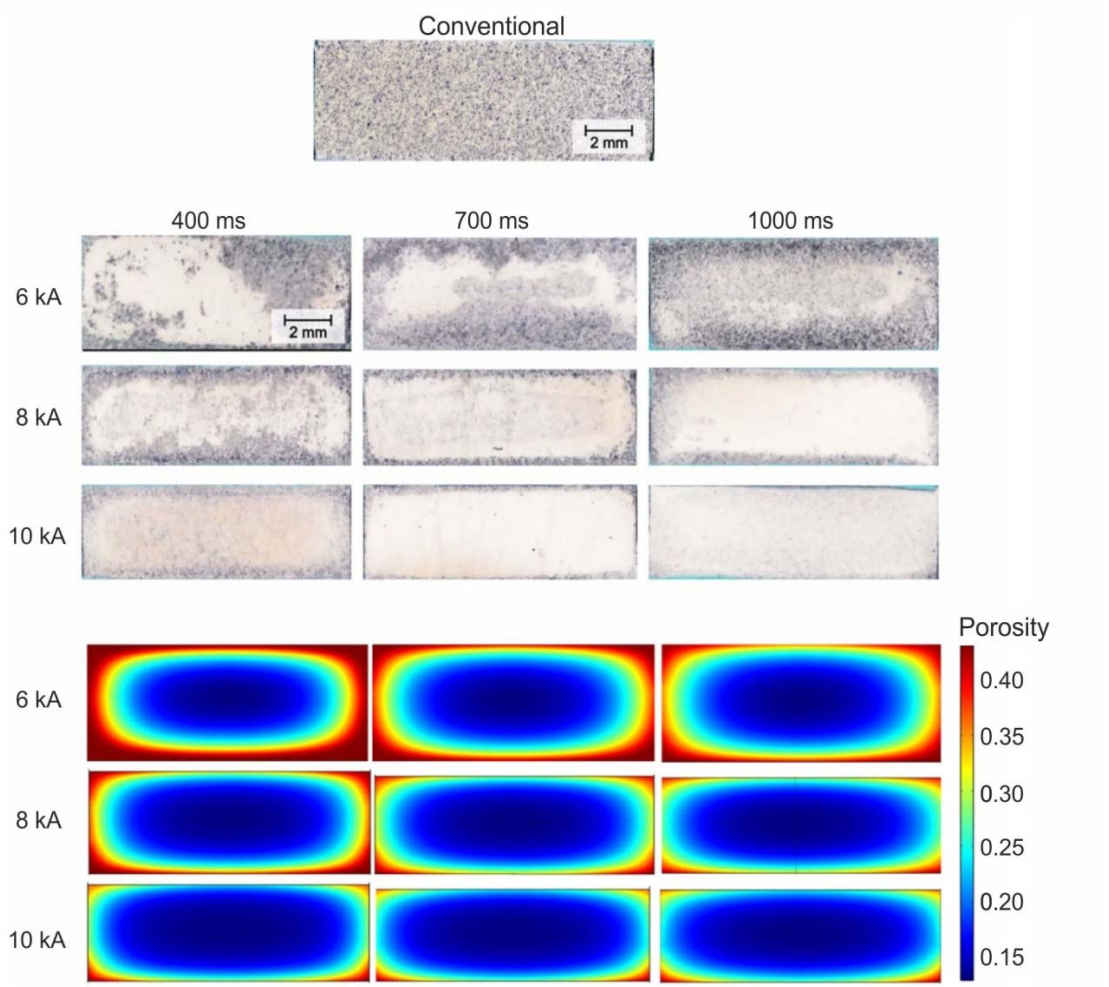

Figure 5. Porosity distribution in a conventionally consolidated specimen (top) and in the different MF-ERS Fe compacts (middle). White areas (more reflecting) indicate a lower porosity content. The same simulated porosity distribution, in color maps (bottom).

Even more interesting is the temperature distribution at any moment during the process. This information is only accessible with the model prediction, but not in an experimental way. Therefore, regarding the temperature, predictions cannot be experimentally confirmed, but the simulation can help understanding the obtained results in the experiences. Fig. 6 shows the temperature distribution in the final instant of a typical experience.

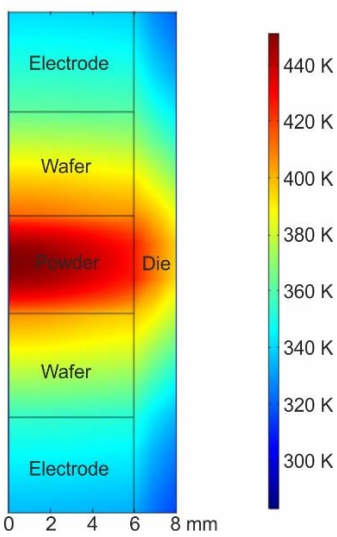

Figure 6. Simulation of the color map representing the temperature distribution in the system (including powder, wafers, and a portion of the electrodes and die) at the end of the process for a MF-ERS Fe compact consolidated with 8 kA and 700 ms.

As easily deduced from a simple comparison of Figs. 5 and 6, the porosity distribution in the compact is due to a fairly similar temperature distribution. The temperature prediction does not only concern the powder, but the whole system. In this respect, the maximum temperatures reached by the wafers and the die are particularly important for determining their durability.

It is worth noting that the maximum temperature reached in the experiences, in the center of the powder mass, can be quite high under extreme processing conditions. It is under these conditions when the phase transformations considered through Eq. (7) become important. In this work with Fe powder, the transformation from bcc to fcc structure has been considered in those areas of the material with a temperature higher than 912 ºC.

4.2. Influence of the current intensity

An expected result in MF-ERS experiments is the increase of densification for higher current intensities and heating times. It will be now analyzed the global porosity and the mean temperature evolution for different current intensities (6, 8 and 10 kA) and the same heating time and applied pressure of 100 MPa. The mean global porosity and temperature are the integral average of the respective local variables in the whole domain of the powder mass at each instant. Graphs in Fig. 7 show the experimental and simulated global porosity evolution in all the MF-ERS experiences. On the other hand, Fig. 8 shows the mean temperature evolution.

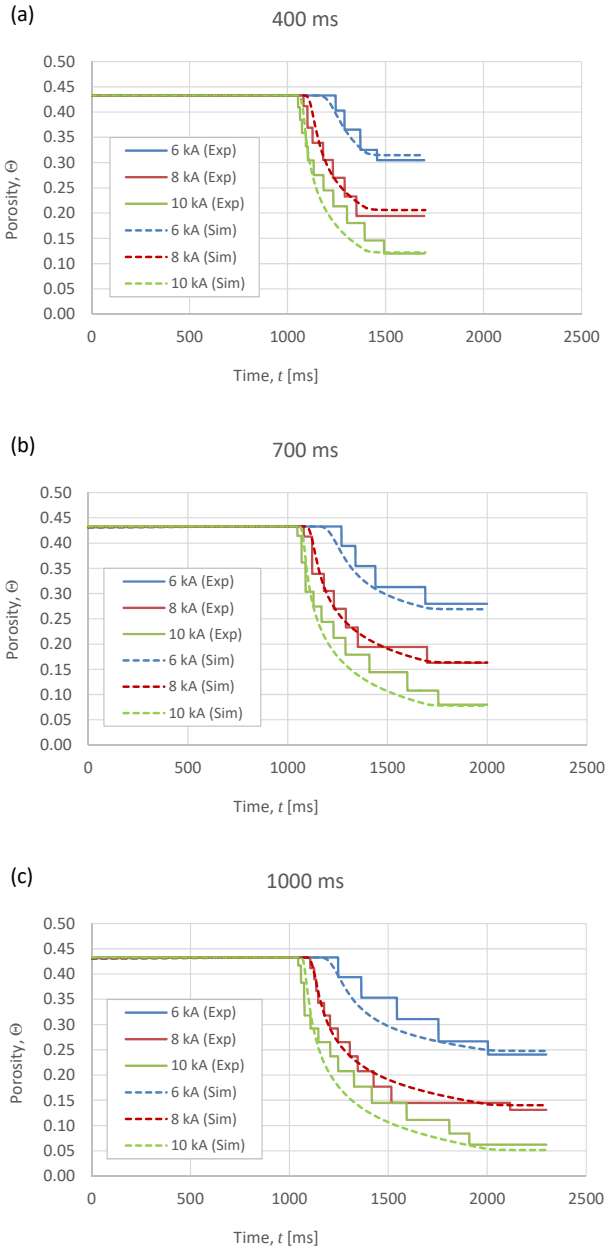

Figure 7. Evolution of the global porosity Θ, as a function of the current intensity, for different heating times: a) 400 ms, b) 700 ms and c) 1000 ms. (The serrated shape of the experimental curve is a consequence of the noise reduction function of the displacement sensor.)

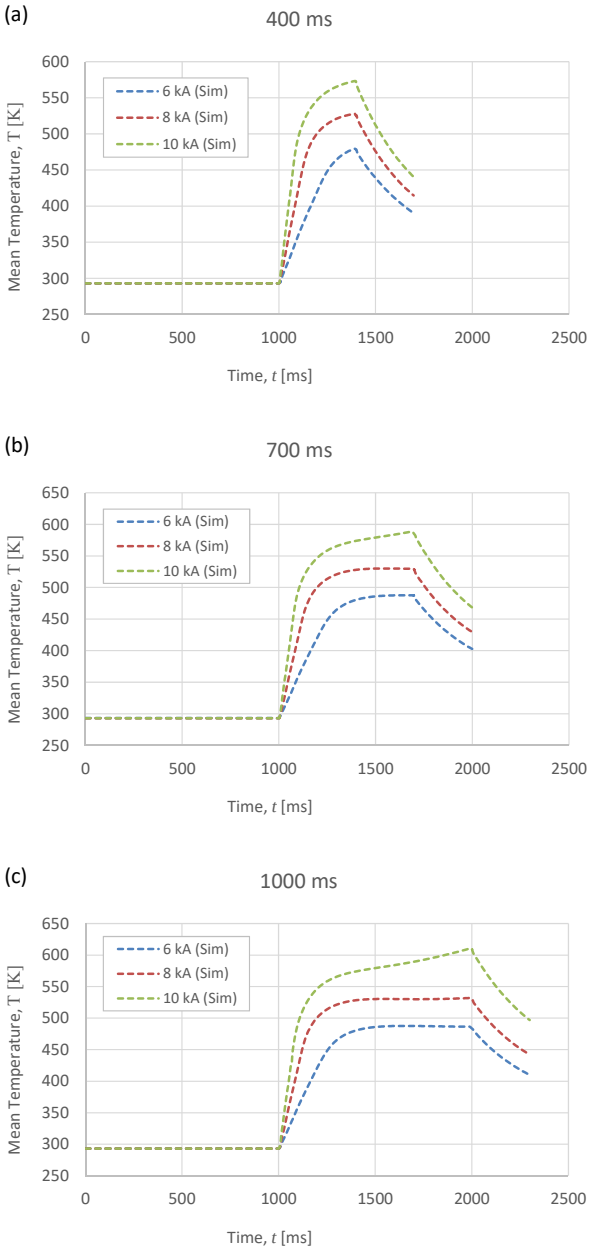

Figure 8. Evolution of the mean temperature T of the powder mass, as a function of the current intensity, for different heating times: a) 400 ms, b) 700 ms and c) 1000 ms.

As can be seen in Fig. 7, predictions of the porosity evolution are satisfactorily validated by comparison with experimentally acquired curves. It is also observed how the final porosity is markedly reduced by increasing the current circulating through the powder mass. However, the relationship between intensity and porosity is not linear, because as can be seen in Eq. (17), the square of the intensity intervenes in formula of the generated thermal energy, and also the electrical resistance, therefore resulting a complicated relationship that can only be understood

with the η value. On the other hand, higher intensities clearly make the porosity to start decreasing earlier, as a consequence of the higher reached temperature and greater softening of the powder.

Fig. 8 shows that the higher the intensity, the higher the temperature increase rate and the temperature reached. The increase of the dwelling time does not seem to be translated into a significant increase in the mean temperature, but into the extension (in the form of a plateau) of the time spent at the maximum temperature. Thus, the increase of the heating time should result in a greater microstructural uniformity of the compact obtained.

Predictions about the evolution of the mean temperature cannot be experimentally contrasted, but those corresponding to the mean porosity can. Simulated macrographs in Fig. 5 seem to show a higher microstructural uniformity inside the compacts by increasing the passage time for a given current intensity, which confirms the simulator predictions. The good agreement of these predictions gives some confidence about the temperature estimations offered by the simulator.

4.3. Influence of the heating time

It is also interesting to compare the overall porosity and mean temperature evolution obtained for different heating times (400, 700 and 1000 ms) and the same current intensity and pressure. Fig. 9 shows the evolution of the global porosity. As can be seen at a glance, the influence of the heating time is much lower than the influence of the current intensity. On the other hand, Fig. 10 shows the evolution of the mean temperature. Again, the influence of the heating time is lower than the influence of the current intensity. It is worth noting that, as expected, for a particular intensity, simulated curves overlap up to the moment that current intensity stops passing through the powder mass. However, this is not the case for the experimental porosity curves. This confirms the stochastic character of all the powder metallurgical processes. This stochastic character has obviously not been considered in the model, although could be easily done through a Gaussian noise generator.

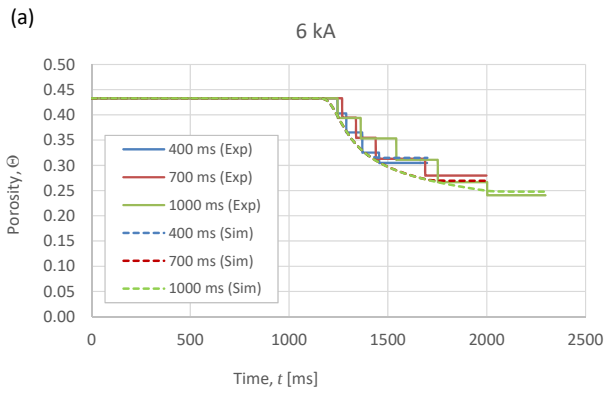

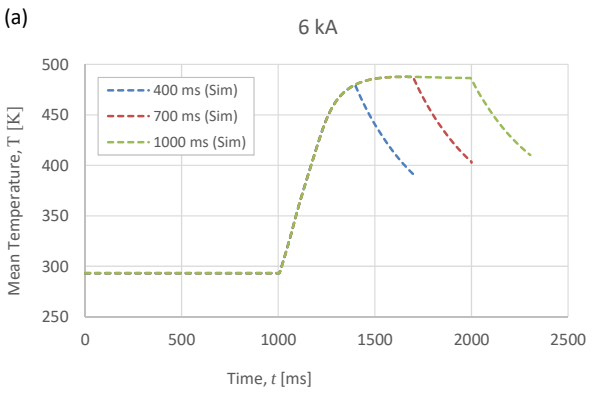

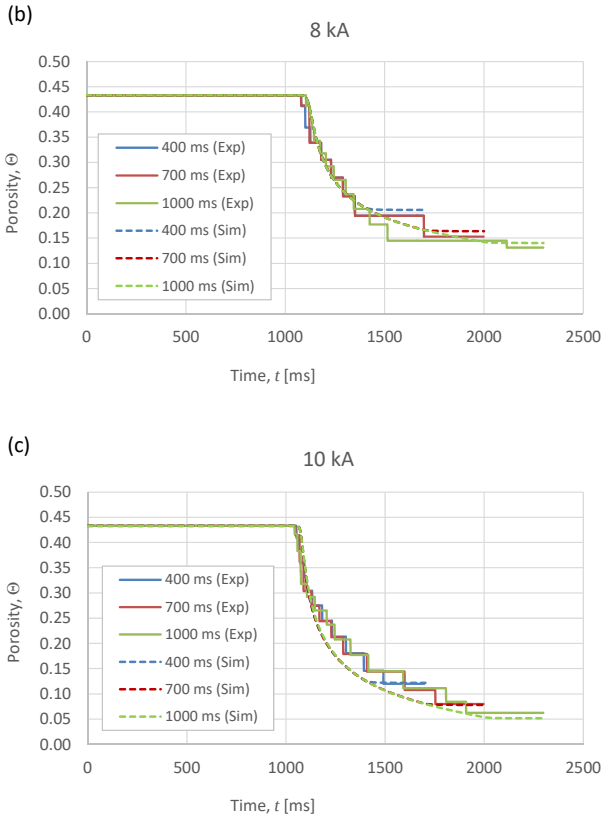

Figure 9. Evolution of the global porosity Θ, as a function of the heating time, for different current intensities: a) 6 kA, b) 8 kA and c) 10 kA.

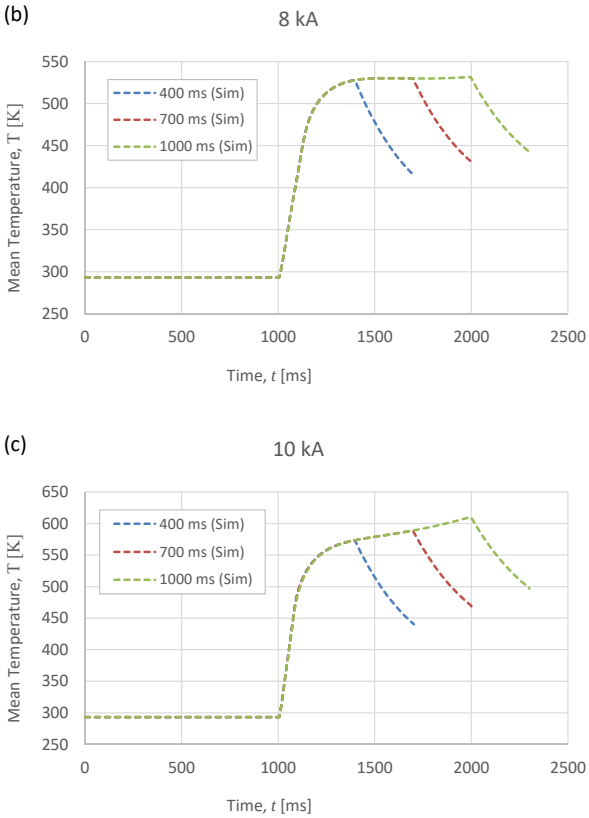

Figure 10. Evolution of the mean temperature T of the powder mass, as a function of the heating time, for different current intensities: a) 6 kA, b) 8 kA and c) 10 kA.

As shown in Fig. 9 and Fig. 10, for 6 and 8 kA, once heating starts, the maximum mean temperature is reached in about 500 ms, although the porosity does not stop decreasing. It is also observed that the maximum mean temperature remains virtually constant for different heating times. However, a different behavior is observed for 10 kA: the mean temperature continues increasing until the final of the heating period. This different behavior for experiments carried out with 6 and 8 kA is possibly due to the fact that the porosity reduction makes the powder resistivity to decrease and the thermal conductivity to increase, therefore releasing less heat, and making possible to evacuate more heat. Thus, time does not affect the mean temperature, being reached an equilibrium value. On the other hand, the much bigger amount of thermal energy released with 10 kA, cannot be compensated by the porosity reduction effect.

4.4. Influence of the pressure

The evolution of the mean temperature and mean porosity for different applied pressures (100 and 200 MPa) are now compared. This is done for arbitrarily selected conditions, in particular for a heating intensity of 8 kA and a heating time of 700 ms.

As can be seen in Fig. 11, when the pressure is increased, the mean temperature of the powder mass decreases and, therefore, the final porosity values are slightly higher.

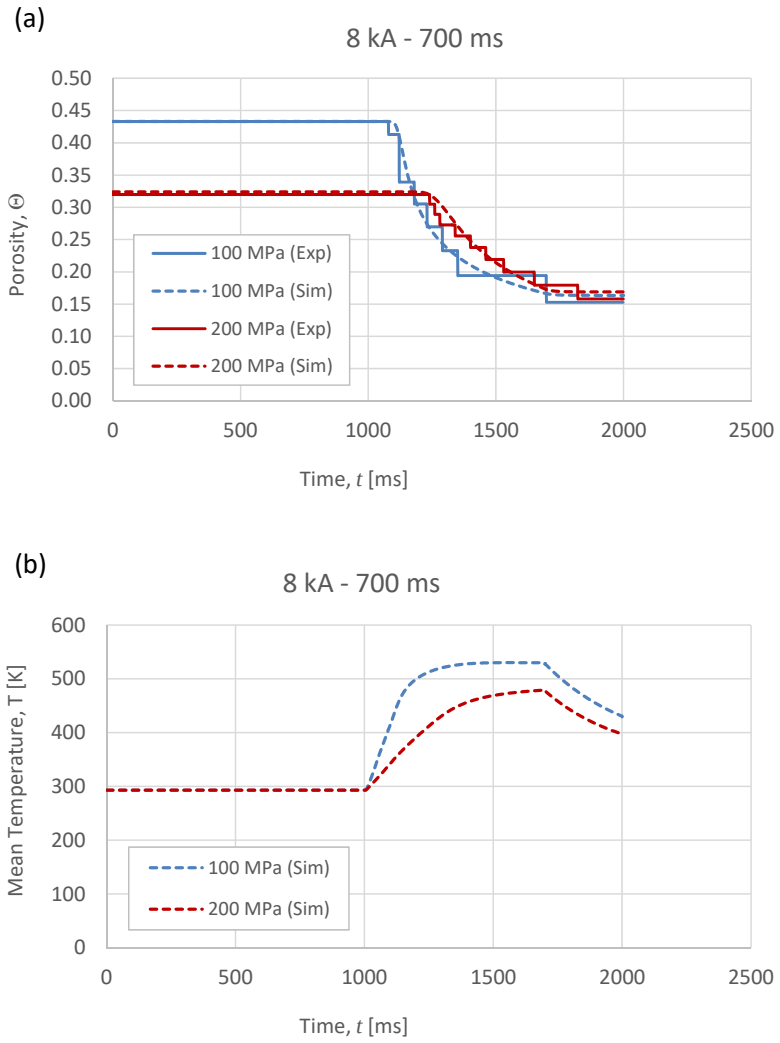

Figure 11. Evolution of a) the overall porosity and b) the mean temperature of the powder mass, of 8 kA and 700 ms compacts processed with pressures of 100 MPa and 200 MPa.

Again, the mean temperature evolution prediction is not contrastable with experimental data. This is only possible for the porosity evolution, as shown in Fig. 11a. The concordance is quite good for both experiences, despite the values of the parameters A_c and n_c were optimized for a target curve obtained from an experience with 100 MPa and not 200 MPa.

However, the most important thing is that the experimental and theoretical curves coincide, with both experiences resulting in a practically identical final porosity. Thus, higher pressures result in lower porosities after the cold-pressing stage, and, contrarily to expected, lower porosities result counterproductive for the subsequent densification during the heating stage. The lower porosity at the beginning of this stage means that the resistivity of the powder mass is lower and,

therefore, the thermal energy released by the Joule effect for a particular current intensity will also be lower.

4.5. Influence of the die material

It is now compared the evolution of the mean porosity and mean temperature of the powder mass using two different materials for the ceramic die containing the powder during the MF-ERS experiences. The two considered materials are alumina and sialon, with thicknesses of 2 mm. The arbitrarily chosen test conditions were: current intensity of 8 kA, heating time of 700 ms and pressure of 100 MPa.

The evolution of the mean porosity and mean temperature obtained with simulations, and experimentally confirmed for the porosity, are shown in Fig. 12.

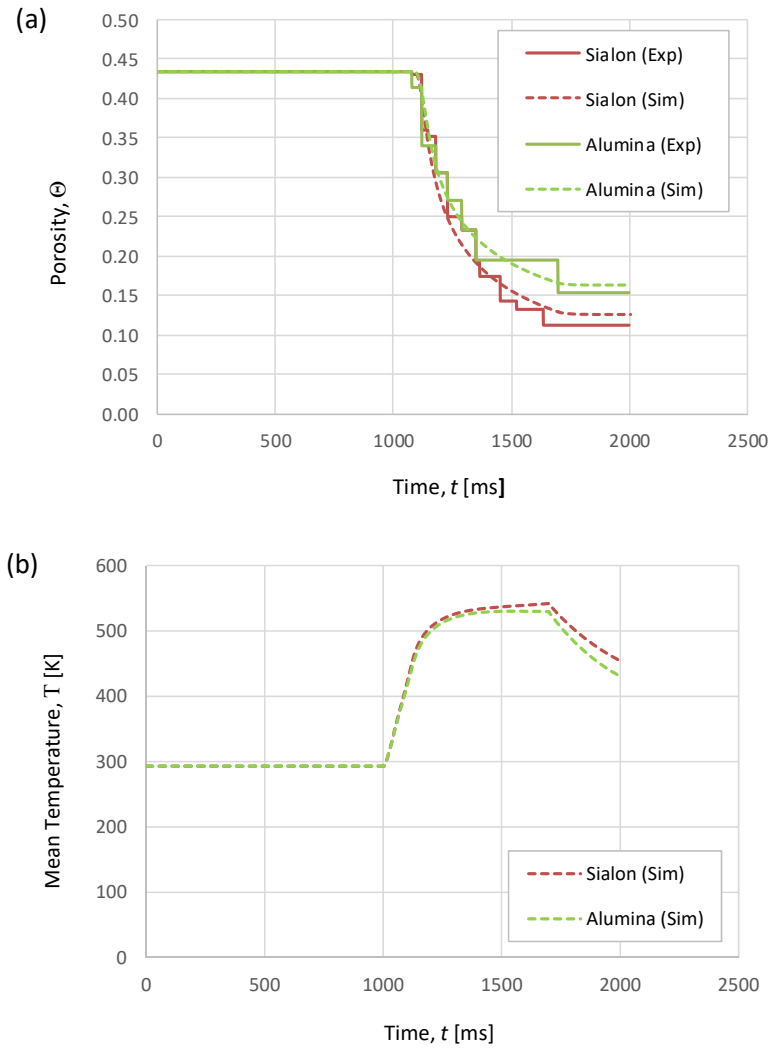

Figure 12. Evolution of: (a) global porosity and (b) mean temperature of the powder mass, for different die materials.

Because sialon is a worse thermal conductor than alumina, the amount of heat dissipated through the die walls in contact with powders is lower for sialon. Therefore, the mean temperature of the powder mass for the sialon die (as shown in Fig. 12b) is always slightly higher. These differences are clearer for higher times, with the curves following an almost parallel behavior, but not great differences are observed at the beginning of the experience. In the same sense, it is understood that the mean porosity is always somewhat lower for the sialon die (Fig. 12a).

On the other hand, the choice of one or other material does not change the instant in which porosity begins to fall, and neither the instant in which the maximum temperature value is reached.

Although previous mean values in the whole powder mass show certain differences, it is expected to find higher differences near the contact with the die.

5. Conclusions

A model of the MF-ERS process has been proposed. The softening due to the heat released by the Joule effect of the electric current passing through the powder mass under pressure has been considered as the only densification mechanism. The inherent sintering rate as well as any other phenomena (including the controversial plasma generation) have been neglected. The constitutive equations modelling the behaviour of the powder mass depend not only on its degree of porosity, but also on certain morphometric parameters of the powder, gathered through the value of the tap porosity of the initial powder.

The MF-ERS model proposed has been successfully validated. After selecting by the least square regression method two fitting parameters (A_c and n_c), the evolution of global quantities such as the porosity and the temperature have been faithfully obtained for the chosen experimental conditions. Once fixed, the values of the fitting parameters also give a good prediction of the evolution of these global magnitudes under different heating conditions (intensity, heating time and pressure).

The predicted porosity distribution reasonably agrees with the experimental observations. Regarding the temperature predictions, it is not possible to have experimental corroboration, however obtaining logical and expected results from the simulations. Although the values of the free parameters (A_c and n_c) were set for a particular working pressure, it was shown that the predictions were still reasonably good for a higher working pressure. These predictions corroborate the experimental result showing that, with this technique, increasing pressure does not necessarily yields to a decrease in the final porosity of the compact.

Finally, the effect of the thermal conductivity of the die material has also been correctly predicted and the theoretical porosity distributions fit reasonably well with those observed experimentally.

Acknowledgements

The authors grateful to FEDER/MEyC, Madrid, for funding this research within the framework of Projects DPI2015-69550-C2-1-P and DPI2015-69550-C2-2-P. The authors also wish to thank the technicians J. Pinto, M. Madrid and M. Sanchez (Univ. Seville) for experimental assistance.

References

[1] S. Grasso, Y. Sakka, G. Maizza, *Electric current activated/assisted sintering (ECAS): a review of patents 1906–2008*, Sci. Technol. Adv. Mater. 10(5) (2009) 1-24

[2] J. Lux, *Improved Manufacture of Electric Incandescent Lamp Filaments from Tungsten or Molybdenum or an Alloy Thereof*, GB Patent 27.002 (1906)

[3] G. Weintraub, H. Rush, *Process and apparatus for sintering refractory materials*, US Patent 1.071.488A, (1913)

[4] G.F. Taylor, *Apparatus for Making Hard Metal Compositions*, US Patent 1.896.854 (1933)

[5] F.V. Lenel, *Resistance Sintering Under Pressure*, JOM 7(1) (1955) 158-167

[6] G. Lee, M.S. Yurlova, D. Giuntini, E.G. Grigoryev, O.L. Khasanov, J. McKittrick, E.A. Olevsky, *Densification of zirconium nitride by spark plasma sintering and high voltage electric discharge consolidation: A comparative analysis*, Ceramics International 41 (2015) 14973-14987

[7] I. Bogachev, A. Yudin, E. Grigoryev, I. Chernov, M. Staltsov, O. Khasanov, E. Olevsky, *Microstructure Investigation of 13Cr-2Mo ODS Steel Components Obtained by High Voltage Electric Discharge Compaction Technique*, Materials 8 (2015) 7342-7353

[8] M. Dzmitry, B. Klimenty, *A porous materials production with an electric discharge sintering*, Int. Journal of Refractory Metals and Hard Materials 59 (2016) 67-77

[9] A. Darvizeh, M. Alitavoli, N. Namazi, *An investigation into the parameters affecting the breakdown voltage and inter-particle bonding in the electrical discharge compaction of metal powders*, Advanced Powder Technology 29 (2018) 2346-2355

[10] R. Orrù, R. Licheri, A.M. Locci, A. Cincotti, G. Cao, *Consolidation/synthesis of materials by electric current activated/assisted sintering*, Mat. Sci. Eng. R 63(4-6) (2009) 127-287

[11] O. Guillon, J. Gonzalez-Julian, B. Dargatz, T. Kessel, G. Schierning, J. Räthel, M. Herrmann, *Field-Assisted Sintering Technology/Spark Plasma Sintering: Mechanisms, Materials, and Technology Developments*, Advanced Engineering Materials 16(7) (2014) 830-849

[12] E.A. Olevsky, E.V. Aleksandrova, A.M. Ilyina, D.V. Dudina, A.N. Novoselov, K.Y. Pelve, E.G. Grigoryev, *Outside Mainstream Electronic Databases: Review of Studies Conducted in the USSR and Post-Soviet Countries on Electric Current-Assisted Consolidation of Powder Materials*, Materials 6(10) (2013) 4375-4440.

[13] T.I. Istomina, A.A. Baidenko, A.I. Raichenko, M.A. Goldberg, A.V. Svechkov, *Influence of premolding pressure in electric discharge sintering on the physicomechanical properties of a copper-tin-abrasive composite*, Sov. Powder Metall. Met. Ceram. 22(11) (1983) 957-960

[14] V.V. Meshkov, N.K. Myshkin, A.I. Sviridenko, *Method of calculating the process parameters of the electric-discharge sintering of conducting powders*, Sov. Powder Metall. Met. Ceram. 23(3) (1984) 200-203

[15] A.I. Raichenko, *Theory of metal powder sintering by an electric-pulse discharge*, Sov. Powder Metall. Met. Ceram. 24(1) (1985) 26-30

[16] G.L. Burenkov, A.I. Raichenko, A.M. Suraeva, *Dynamics of interparticle reactions in spherical metal powders during electric sintering*, Sov. Powder Metall. Met. Ceram. 26(9) (1987) 709-712

[17] A.I. Raichenko, E.S. Chernikova, *A mathematical model of electric heating of the porous medium using current-supplying electrode/punches*, Sov. Powder Metall. Met. Ceram. 28(5) (1989) 365-371

[18] G.L. Burenkov, A.I. Raichenko, A.M.Suraeva, *Macroscopic mechanism of formation of interparticle contact in electric current sintering of powders*, Sov. Powder Metall. Met. Ceram. 28(3) (1989) 186-191

[19] M. Yoneya, T. Ikeshoji, *A numerical calculation method advantageous for complex boundary problems: an application to the pulse discharge sintering process*, Mater. Trans. 42(11) (2001) 2165-2171

[20] K. Matsugi, H. Kuramoto, T. Hatayama, O. Yanagisawa, *Temperature distribution at steady state under constant current discharge in spark sintering process of Ti and Al2O3 powders*, J. Mater. Process. Technol., 134(2) (2003) 225-232

[21] U. Anselmi-Tamburini, S. Gennari, J.E. Garay, J.R. Groza, Z.A. Munir, *Fundamental investigations on the spark plasma sintering/synthesis process*, Mater. Sci. Eng. A 394(1-2) (2005) 139-148

[22] E. Olevsky, L. Froyen, *Constitutive modeling of spark-plasma sintering of conductive materials*, Scripta Mater. 55(12) (2006) 1175-1178

[23] X. Wang, G. Casolco, G. Xu, J.E. Garay, *Finite element modeling of electric current-activated sintering: the effect of coupled electrical potential, temperature and stress*, Acta Mater. 55(10) (2007) 3611-3622

[24] J. Zhang, *Field Activated Sintering Technology: Multi-physics Phenomena Modeling. A coupled thermal-electrical-densification framework*, LAP LAMBERT Academic Publishing AG & Co. KG, 2010

[25] E.A. Olevsky, W.L. Bradbury, C.D. Haines, D.G. Martin, D. Kapoor, *Fundamental Aspects of Spark Plasma Sintering: I. Experimental Analysis of Scalability*, J. Am. Ceram. Soc. 95 (2012) 2406-2413

[26] Z.A. Munir, D.V. Quach, M. Ohyanagi, *Electric current activation of sintering: a review of the pulsed electric current sintering process*, J. Am. Ceram. Soc. 94(1) (2011) 1-19

[27] E.A. Olevsky, C. Garcia-Cardona, W.L. Bradbury, C.D. Haines, D.G. Martin, D. Kapoor, *Fundamental aspects of spark plasma sintering: II. Finite element analysis of scalability*, J. Am. Ceram. Soc. 95 (2012), 2414-2422

[28] J.M. Montes, F.G. Cuevas, J. Cintas, P. Urban, *A One-Dimensional Model of the Electrical Resistance Sintering Process*, Met. Mater. Trans. A 46 (2015), 963-980

[29] MPIF Standard 4, *Determination of Apparent Density of Free-Flowing Metal Powders Using the Hall Apparatus*, in: Standard test methods for metal powders and powder metallurgy products, MPIF, Metal Powder Industries Federation, Princeton, NJ, USA, 2016

[30] R.M. German, *Particle packing characteristics*, MPIF (Metal Powders Industries Federation), Princeton, New Jersey, 1989

[31] J.M. Montes, J.A. Rodríguez, E.J. Herrera, *Thermal and electrical conductivities of sintered powder compacts*, Powder Metallurgy 46(3) (2003) 251-256

[32] J.M. Montes, F.G. Cuevas, J.A. Rodríguez, E.J. Herrera, *Electrical conductivity of sintered powder compacts*, Powder Metallurgy 48(4) (2005) 343-344

[33] J.M. Montes, F.G. Cuevas, J. Cintas, *Electrical and thermal tortuosity in powder compacts*, Granular Matter 9 (2007) 401-406

[34] J.M. Montes, F.G. Cuevas, J. Cintas, *Porosity effect on the electrical conductivity of sintered powder compacts*, Applied Physics A: Materials Science and Processing 92 (2008) 375-380

[35] J.M. Montes, F.G. Cuevas, J. Cintas, S. Muñoz, *Thermal Conductivity of Powder Aggregates and Porous Compacts*, Met. Mat. Trans. A. 43(12) (2012) 4532-4538

[36] J.M. Montes, F.G. Cuevas, J. Cintas, J.M. Gallardo, *Electrical conductivity of metal powder aggregates and sintered compacts*, J. Mater. Sci., 51 (2016) 822-835

[37] MPIF Standard 46, Determination of tap density of metal powders, in: Standard test methods for metal powders and powder metallurgy products, MPIF, Metal Powder Industries Federation, Princeton, NJ, USA, 2016.

[38] J.M. Montes, F.G. Cuevas, J. Cintas, *Electrical resistivity of metal powder aggregates*, Metallurgical and Materials Transactions B: Process Metallurgy and Materials Processing Science 38(6) (2007) 957-964

[39] J.M. Montes, F.G. Cuevas, J. Cintas, P. Urban, *Electrical conductivity of metal powders under pressure*, Applied Physics A: Materials Science and Processing 105(4) (2011), 935-947

[40] J.M. Montes, F.G. Cuevas, J. Cintas, F. Ternero, E.S. Caballero, *Electrical Resistivity of Powdered Porous Compacts*, in: Electrical and Electronic Properties of Materials, Ed. by Md. Kawsar Alam, IntechOpen, London, UK, 2018

[41] T.J. Garino, *Electrical behavior of oxidized metal powders during and after compaction*, J. Mater. Res. 17(10) (2002) 2691-2697

[42] L.P. Lefebvre, G. Pleizier, Y. Deslandes, *Electrical resistivity of green powder compacts*, Powder Metall. 44(3) (2001) 259-266

[43] L.I. Cheng-Feng, Z.H.U. Shen-Gang, *Apparent electrical conductivity of porous titanium prepared by the powder metallurgy method*, Chin. Phys. Lett. 22 (10) (2005) 2647-2650

[44] N. Tsuda, K. Nasu, A. Fujimori, K. Siratori, *Electronic Conduction in Oxides*, 2nd ed., Springer-Verlag, Berlin, Germany, 2000.

[45] J.M. Montes, F.G. Cuevas, J. Cintas, R. Sepúlveda, *Modelling of three powder compaction laws for cold die pressing*, International Journal of Materials Research 103(12) (2012) 1444-1454

[46] J.M. Montes, F.G. Cuevas, J. Cintas, F. Ternero, E.S. Caballero, *On the Compressibility of Metal Powders*, Powder Metall. 61(3) (2018) 219-230

[47] J. Secondi, *Modelling powder compaction: From a pressure-density law to continuum mechanics*, Powder Metall. 45(3) (2002) 213-217

[48] MPIF Standard 45, Method for Determination of Compressibility of Metal Powders, in: Standard test methods for metal powders and powder metallurgy products, MPIF, Metal Powder Industries Federation, Princeton, NJ, USA, 2016

[49] J.M. Montes, F.G. Cuevas, J. Cintas, F. Ternero, E.S. Caballero, *On the densification kinetics of metallic powders under hot uniaxial pressing*, Metals and Materials International (in press, DOI: 10.1007/s12540-018-00216-9)

[50] R.W. Evans, B. Wilshire, *Introduction to creep*, The Institute of Materials, London, UK, 1993

[51] A.N. Tijonov, A.A. Samarski, *Ecuaciones de la Física Matemática*, 2nd ed., MIR, USSR, 1980. (in Spanish)

[52] R. Haberman, *Elementary applied partial differential equations*, Prentice-Hall International Inc, Englewood Cliffs, New Jersey, USA, 1987

[53] F. P. Incropera, D.P. DeWitt, T.L. Bergman and A.S. Lavine: *Fundamentals of Heat and Mass Transfer*, 6th ed., Wiley John & Sons, USA, 2006

[54] Smithells metals reference book, 8th ed., Gale, W.F., Totemeier, T.C. (Eds.), Elsevier Butterworth-Heinemann Ltd, Oxford, UK, 2004

[55] ASM Handbook, Vol. 2, *Properties and selection: nonferrous alloys and special purpose materials*, ASM International, USA, 1990, pp. 1099-1201.

[56] CRC Handbook of Chemistry and Physics, 80th ed., CRC Press, New York, USA, 1999-2000.